Assessment of the Mixing Procedure and the Effect of Carboxylated Nitrile Rubber as a Compatibilizer for Kraft Lignin/Nitrile Rubber Composites

Nicoly Rosario da Costa, Gustavo Ninho Campos, Elisson Brum Dutra da Rocha, João Paulo Cosas Fernandes, Ana Maria Furtado de Sousa

SPE Polymers

WILEY | spe INSPIRING PLASTICS PROFESSIONALS

RESEARCH ARTICLE OPEN ACCESS

Assessment of the Mixing Procedure and the Effect of Carboxylated Nitrile Rubber as a Compatibilizer for Kraft Lignin/Nitrile Rubber Composites

Nicoly Rosario da Costa[1] | Gustavo Ninho Campos[1,2] | Elisson Brum Dutra da Rocha[1] | João Paulo Cosas Fernandes[2] | Ana Maria Furtado de Sousa[1]

[1]Chemistry Institute, Rio de Janeiro State University, Rio de Janeiro, Rio de Janeiro, Brazil | [2]Univ. Grenoble Alpes, CNRS, CERMAV, Grenoble, France

Correspondence: Nicoly Rosario da Costa (nicolyrc17@gmail.com)

Received: 3 December 2025 | **Revised:** 19 December 2025 | **Accepted:** 21 December 2025

Keywords: composite | filler | lignin | rubber

ABSTRACT

The growing interest in sustainable rubber materials motivates the use of renewable resources for the development of advanced materials. Lignin, valued for its abundance, biodegradability, and mechanical strengths, emerges as a promising alternative filler in rubber composites. This study produced composites using nitrile rubber (NBR) and a 70:30 blend of NBR with carboxylated nitrile rubber (XNBR), each incorporating 40 parts per hundred of rubber (phr) of kraft lignin. Two methods were tested for incorporating lignin: direct addition of 40 phr of lignin powder to the rubbers or compounding using masterbatches of NBR/lignin and XNBR/lignin, each with 130 phr of lignin produced by co-coagulation. Results revealed that NBR/XNBR/lignin composites show thinner, more aligned lignin particles than NBR/lignin composites, with the masterbatch technique further reducing particle size. All lignin-filled rubbers exhibited an increased reaction rate constant of vulcanization, lower covalent crosslink density, and higher ionic crosslink density compared to unfilled rubber. Notably, composites made with lignin masterbatch exhibited a reduced Payne effect, as well as higher tensile and tear strengths, than those made using lignin powder. These findings suggest that incorporating lignin via a masterbatch and blending with XNBR offers a compelling strategy for enhancing the properties of NBR-based rubber composites.

1 | Introduction

In recent years, the need for environmental awareness and sustainable practices has gained the attention of researchers and industries around the world. The consumption of fossil fuels has increased considerably with the development and population growth, and with it, the associated environmental issues, ranging from pollution to global warming. The search for greener and more sustainable alternatives for both energy sources and materials has received considerable attention in response. One area of emphasis in this theme involves the development of composites based on fillers of natural and renewable origin, replacing non-renewable fossil sources [1, 2].

The method of reinforcing rubbers by applying fillers has been essential in fulfilling market needs across multiple sectors, including sealing components, hoses, tires, and footwear. Carbon black (CB) is used as a major reinforcing filler in the rubber industry. However, CB manufacture has a significant influence on greenhouse gas emissions, and its non-renewable source, oil, has prompted the quest for environmentally viable alternatives to replace its use as reinforcement in elastomeric materials [3].

Highlights

- XNBR enhances lignin elongation and dispersion in rubber.
- Masterbatch method reduces lignin agglomerate size significantly.
- Masterbatch method enhances tensile strength over powder method.
- Lignin increases vulcanization rate constant and reaction order.
- Lignin reduces covalent crosslinks but increases ionic crosslinks.

In this regard, renewable-based fillers such as lignin, cellulose nanofibers, starch, and eggshell have been investigated as rubber composite reinforcement candidates [4, 5].

Lignin is the second most abundant biopolymer on Earth, after cellulose, and it composes 15%–36% of plant cell walls. Lignin possesses several attractive properties, including high carbon content, biodegradability, antioxidant activity, and rigidity, which have sparked interest in the development of materials with greater added value. Potentially, its use in the composition of materials could help in resolving issues related to the depletion of natural resources and global warming. However, despite the broad perspectives it offers, less than 2% of the lignin produced is directed to products with higher added value, such as stabilizers, concrete additives, surfactants, and dispersants. The remainder is used as low-quality fuel. Furthermore, the difficulty of compatibility with other polymeric systems limits the success of creating high-performance polymer-based materials with lignin [2–4, 6].

Among the different types of technical lignins, kraft lignin is the most widely produced, as it is obtained as a by-product of the kraft pulping process. Its chemical structure is rich in phenolic and aliphatic hydroxyl groups, as well as carbonyl functionalities, which confer a pronounced polar character and antioxidant activity [7]. While these functional groups provide opportunities for chemical interactions with polar elastomers, they also contribute to poor compatibility and dispersion when Kraft lignin is incorporated into nonpolar rubber matrices.

Mohamad Aini et al. [8] examined the findings of various studies regarding the performance of rubber composites that incorporate lignin as a reinforcing filler. This review highlights that achieving compatibilization between rubber and lignin presents a considerable challenge, primarily due to the polar characteristics of lignin in contrast to the nonpolar properties of various rubbers, including natural rubber (NR) and styrene-butadiene rubber (SBR). The incompatibility leads to poor dispersion of lignin within the elastomeric matrix, leading to inferior mechanical and thermal properties. To address this issue, various chemical modification techniques and blending methods have been explored.

Studies have explored the use of lignin as a reinforcing agent in rubber composites. Researchers have aimed to enhance properties such as oil resistance, mechanical strength, and thermal stability by modifying lignin and promoting better interaction with the rubber matrix. Li et al. [9] successfully developed a method with chemically modified lignin as a partial substitute for carbon black in NR composites. The addition of ZDMA further enhanced the material's properties by creating a robust, integrated network, resulting in a more sustainable and high-performance composite material with improved lignin compatibility and dispersion in the NR matrix. Sekar et al. [10] investigated the potential of hydrothermally treated (HTT) lignin as a sustainable, bio-based filler for a solution styrene butadiene and butadiene rubber (SSBR/BR) blend compound, comparing its unmodified and silane-modified versions to commercial fillers such as carbon black and precipitated silica. The results indicate that silane-modified HTT lignin exhibits superior in-rubber properties compared to the unmodified version, acting as a semi-reinforcing filler. This improvement is attributed to the formation of a network of HTT lignin particles that traps the rubber or creates sponge-like textures in the presence of a silane coupling agent, highlighting the potential of treated HTT lignin as an alternative, eco-friendly filler for rubber products. However, challenges remain, particularly when using unmodified lignin, which may hinder vulcanization and reduce overall performance. While some improvements have been achieved through chemical treatments, results still fall short of the performance of unfilled rubber, suggesting that further research and optimization are needed.

More recently, studies have explored the interactions of lignin with carboxylated nitrile rubber (XNBR) with promising results [8, 11, 12]. It is hypothesized that zinc oxide forms ionic and metal–ligand coordination interactions between the hydroxyl and carbonyl groups in lignin molecules and the carboxylic groups in XNBR.

Given the importance of enhancing the interaction between lignin and rubber for the development of sustainable and high-performance materials, this study aims to evaluate whether incorporating XNBR as a compatibilizer in the rubber blend can improve the mechanical and rheological properties of NBR/lignin composites. It also investigates how different methods of mixing lignin into the rubber matrix, specifically in masterbatch and powder forms, may affect these properties. By utilizing this compatibilization strategy along with a rubber-lignin masterbatch, we aim to strengthen the interactions between NBR and lignin compounds.

2 | Materials and Methods

2.1 | Materials

Hardwood Kraft Lignin Ecolig (density: 1.4 g/cm^3 and particle size of 1 μm determined by dynamic light scattering) was kindly donated by Suzano Papel e Celulose S.A. The elastomeric materials and vulcanization agents used in this research were kindly donated by Nitriflex S/A. The elastomeric matrices were NBR N615 rubber bale (acrylonitrile content: 31%–34%, Mooney MML1 + 4 viscosity: 42–52), NBR N615 rubber latex aqueous suspension (acrylonitrile content: 31%–34%, Mooney MML1 + 4 viscosity: 42–52, solids content 26.2%, pH 9.60), and

XNBR N3330X rubber latex aqueous suspension (acrylonitrile content: 31%–34%, Mooney MML1 + 4 viscosity: 42–52, carboxylic acid content: 7%, solids content 28.5%, pH 7.64). The vulcanization agents used were zinc oxide, stearic acid, sulfur, 2-mercaptobenzothiazole (MBTS), and tetramethyl thiuram disulfide (TMTD). The coagulant bath formulations for N615 latex (pH 3.3) and for N3330X latex (pH 6.5) cannot be described for reasons of confidentiality.

2.2 | Experimental Part Description

2.2.1 | Preparation of an Aqueous Lignin Suspension

435 g of distilled water at 29°C (room temperature) and 148 g of Kraft lignin were initially weighed and then transferred into a 1 L beaker. The mixture was stirred with an Ika Ultra-turrax disperser at 17,500 rpm for 10 min, resulting in an aqueous lignin suspension with a total solids content of 25%. A total of four batches were produced, each with a pH of 2.

2.2.2 | Co-Coagulation Step to Yield NBR/Lignin and XNBR/Lignin Masterbatches With 135 phr of Lignin

The lignin suspension and latex were mixed and left under constant agitation for 30 min. Then, the mixtures of latex/lignin were co-coagulated under intense stirring in a metal vessel with a coagulant bath (according to the type of latex). The particles were separated by filtration, vigorously washed with running water until all residual bath was completely removed, and dried in an air-circulating oven at 100°C for 1 h. Further, the unfilled NBR latex and XNBR latex were also coagulated using the same protocol. The overall yield of the procedure was as follows: XNBR/Lignin: 69%, NBR/Lignin: 69%, XNBR: 98%, and NBR: 91%. The actual amounts in phr of lignin incorporated, determined by thermogravimetric analysis (see Figure S1), in each masterbatch were XNBR/Lignin: 129 ± 1 phr and NBR/Lignin: 116 ± 1 phr.

2.2.3 | Preparation of Compounds of NBR/Lignin, Unfilled NBR, and Unfilled NBR/XNBR

Table 1 shows the rubber formulations. The experimental code is "A-B LCD," where "A" and "B" represent the type of rubber ("N" for NBR and "X" for XNBR), "L" is "Lignin," "C" is related to the form in which lignin was added to the composite, that is, "P" for powder lignin or "M" for lignin in a masterbatch, and "D" is the amount of lignin in the composite (0 or 40 parts per hundred of rubber—phr).

All rubber formulations were prepared in a two-roll mixing mill (Luxor, model BML 150) based on the ASTM D3187 mixing protocol and allowed to rest at 25°C for 24 h. Then, each rubber compound was vulcanized at 18 MPa of pressure and 160°C of temperature in sheets (150 × 150 × 2 mm) and cylindrical (28.6 mm in diameter and 12.5 mm in thickness) shapes. The vulcanization times employed were the optimal cure time (t_{90}) for the sheet specimens and t_{90} plus 10 min for the cylinder specimens.

2.3 | Characterization

2.3.1 | Vulcanization Assessment

Rheometric characterization was performed at 160°C, with an arc of ±0.5°C for 30 min, following the ASTM D5289 standard, using a Rubber Processing Analyzer (RPA), model RPA 2000 from Alpha Technologies. Based on the vulcanization curves obtained, the scorch time (t_{s1}), the optimal curing time (t_{90}), and the minimum and maximum torques (ML and MH) of the rubber compounds are established.

The vulcanization kinetics was investigated using the autocatalytic model (Equation 1) [13, 14].

$$\frac{d\alpha}{dt} = k(T)\alpha^m(1-\alpha)^n \quad (1)$$

where $d\alpha/dt$ is a vulcanization rate, α is the vulcanization conversion (or degree of vulcanization), t denotes time (s), $k(T)$ is the reaction rate constant, and m (autocatalytic reaction) and n (non-autocatalytic reaction) are reaction orders. The degree of vulcanization (α) was calculated using Equation (2), where Mt represents the torque in time t [13, 14].

$$\alpha(t) = \frac{(Mt - ML)}{MH - ML} \quad (2)$$

The values of $k(T)$, m, and n were calculated using nonlinear regression analysis using OriginPro4 (student version) software.

TABLE 1 | Compound formulations in parts per hundred of rubbers (phr).

Components	N-N L0	X-N L0	N-N LM40	X-N LM40	N-N LP40	X-N LP40
NBR (bale)	70	70	70	70	70	70
NBR–coagulated	30	—	—	—	30	—
XNBR–coagulated	—	30	—	—	—	30
Lignin (powder)	—	—	—	—	40	40
NBR/Lignin–co-coagulated	—	—	30/40	—	—	—
XNBR/Lignin–co-coagulated	—	—	—	30/40	—	—
Vulcanization system	ZnO: 5 phr, stearic acid: 1 phr, sulfur: 0.5 phr, MBTS: 0.9 phr, and TMTD: 2.5 phr					

2.3.2 | Total, Covalent and Ionic Cross-Link Density Measurement

The apparent cross-link density was determined based on ASTM D297 using the swelling method with organic solvents. First, test specimens of each composition with dimensions of 20 × 20 × 2 mm were weighed in air and subsequently in toluene to calculate their density. The specimens were then immersed in toluene within sealed containers, protected from light, for 1 week until a balance in swollen weight was achieved. Afterward, the swollen samples were removed from toluene and blotted with tissue paper to eliminate excess solvent, followed by immediate weighing. The swollen specimens were allowed to dry for an additional week and were weighed again. The volume of rubber in the swollen state was determined using Equation (3). The apparent cross-link density (CLD) was estimated based on Equation (4), developed for the Flory–Rehner theory, considering the affine model and tetra-functional networks [15].

$$v_r = \frac{\left(\frac{M_1}{\rho_2} - \frac{M_c}{\rho_c}\right)}{\left\{\left(\frac{M_1}{\rho_2} - \frac{M_c}{\rho_c}\right) + \left[\frac{(M_2 - M_3)}{\rho_1}\right]\right\}} \quad (3)$$

$$\mathrm{CLD}\left(\mathrm{mol\,cm^{-3}}\right) = \frac{-\ln(1 - v_r) + v_r + \alpha . v_r^2}{\left[V_0\left(v_r^{\frac{1}{3}} - \frac{v_r}{2}\right)\right]} \quad (4)$$

where v_r is swollen rubber volume at equilibrium, M_1 is sample mass before swelling, M_2 is swollen sample mass, M_3 is dry sample mass after swelling, M_c is filler mass in the sample, ρ_1 is solvent density (0.8623 g mL^{-1}), ρ_2 is sample density, ρ_c is filler density, V_0 is solvent molar volume (106.3 mL) and α is the interaction parameter between the elastomer and the solvent calculated for XNBR/Toluene [16] and NBR/Toluene [17] using Equations (5) and (6), respectively.

$$\alpha = 0.4132 + 0,4341\, vr \quad (5)$$

$$\alpha = 0.3809 + 0,6707\, vr \quad (6)$$

This first determination of apparent cross-link density represents the sum of the covalent and ionic links (apparent total cross-link density). Following the first determination, the specimens were immersed in a mixture of toluene and trichloroacetic acid for 5 days in sealed containers to selectively disrupt the ionic cross-links. The samples were then removed and re-immersed in pure toluene to perform a second determination of cross-link density, following the same swelling protocol used in the first determination of total cross-link density. Since the ionic bonds were disrupted during the toluene and trichloroacetic acid immersion, this second measurement in pure toluene represents only the apparent covalent cross-link density. Finally, the apparent ionic cross-link density was calculated by subtracting the apparent covalent cross-link density (second determination) from the apparent total cross-link density (initial determination) [18]. The cross-link density determination was done in triplicate.

TABLE 2 | Count of lignin particles in SEM photos (20,000 μm² of total area).

Sample	Particles with area > 3 μm²	Particles with area > 20 μm²
N-N LP40	148	52
N-N LM40	138	38
X-N LP40	158	55
X-N LM40	167	38

2.3.3 | Scanning Electron Microscopy

The sample preparation protocols involve cleaning the samples with acetone to eliminate any free residual accelerator (TMTD and MBTS), followed by drying them overnight in a ventilated oven at 60°C. After, all samples were trimmed and surfaced parallel to the thickness direction using a cryo-ultramicrotome (LEICA UC6) at −120°C, ensuring a flat surface for morphological analysis throughout the sheet's thickness. Finally, all samples were coated with gold using a vacuum metallizer. The dispersion of lignin particles in the rubber matrix was assessed by the photos taken with the scanning electron microscope (SEM) FEI QUANTA-FEG 250 equipped with a backscattered electron (BSE) detector. The degree of lignin dispersion was evaluated by counting particles from SEM images using ImageJ software. To better assess the degree of dispersion, the number of lignin particles was quantified by counting particles in SEM images (four photos at a magnification of 2000×, scale bar of 20 μm, total area analyzed per sample: 20,000 μm²) using ImageJ software.

2.3.4 | Rheological Analysis—Payne Effect

The complex shear modulus (G^*) under strain sweep was performed in RPA based on D8059 and D6601 standards. The test protocol consists of four steps: (i) preconditioning for 2 min at 60°C, with a strain of 0.7% and a frequency of 0.1 Hz. This step was needed to ensure the rubber conformation within the grooves, achieve thermal equilibrium, and erase heat history variations prior to testing; (ii) unvulcanized strain sweep at 60°C and 1 Hz, with strain values ranging from 0.7%, 0.9%, 1.1%, 1.3%, 1.7%, 2.1%, 2.6%, 3.2%, 4.0%, 5.0%, 10%, 20%, 30%, 40%, 50%, 60%, 70%, 80%, and 90%; (iii) static vulcanization at 160°C, t_{90}, with a frequency of 0 Hz and 0% strain. These experimental conditions for vulcanization within the RPA are in accordance with dynamic property Condition No. 3 of Table 2 from ASTM D6601 standard; and (iv) vulcanized strain sweep at 60°C and 1 Hz, with strain values ranging from 0.7%, 0.9%, 1.1%, 1.3%, 1.7%, 2.1%, 2.6%, 3.2%, 4.0%, 5.0%, 10%, 20%, 30%, 40%, 50%, 60%, 70%, 80%, and 90%.

The Payne Effect was assessed using data derived from the complex modulus (G^*) curves [19]. The strain range for evaluating the Payne effect was determined to be between 0.7% and 40% (Equation 7), as the complex G^* of unfilled rubber compounds remains strain-independent within this range [19].

$$\text{Payne Effect} = \Delta G^* = G^*_{0.7} - G^*_{40} \quad (7)$$

2.3.5 | Mechanical Properties

Tensile and tear tests were conducted according to ASTM D412 and ASTM D624 standards, respectively, using a universal testing machine (EMIC model DL2000) equipped with a 500 N load cell. The cross-head speed rate was 500 mm min^{-1}, and both analyses were replicated 6 times.

Shore A hardness was measured according to ASTM D2240 using a Shore A durometer Parabor, with 15 measurements performed for each composite.

All statistical analyses of mechanical properties were conducted using Statgraphics Centurion 18, Version 18.1.16, at a 95% confidence level.

3 | Results and Discussion

3.1 | SEM

The mechanical properties of filled vulcanized materials are influenced by both the filler dispersion in the rubber matrix and the adhesion between the rubber and the filler [20]. Figure 1 presents SEM images, captured using a backscattered electron (BSE) detector, illustrating the morphology of the cross-section of the cryo-ultramicrotomed samples. In these images, three distinct phases are identifiable: the rubber matrix (dark gray area), lignin aggregates (light gray particles), and zinc oxide (white dots).

It is observed that both surfaces of N-N L0 (Figure 1a) and X-N L0 (Figure 1d) are smooth, with bright particles, showing the presence of ZnO. The lignin particles in N-N (Figure 1b,c) and X-N (Figure 1e,f) exhibit a lighter contrast compared to the matrix because of the BSE mode used [21]. Overall, all

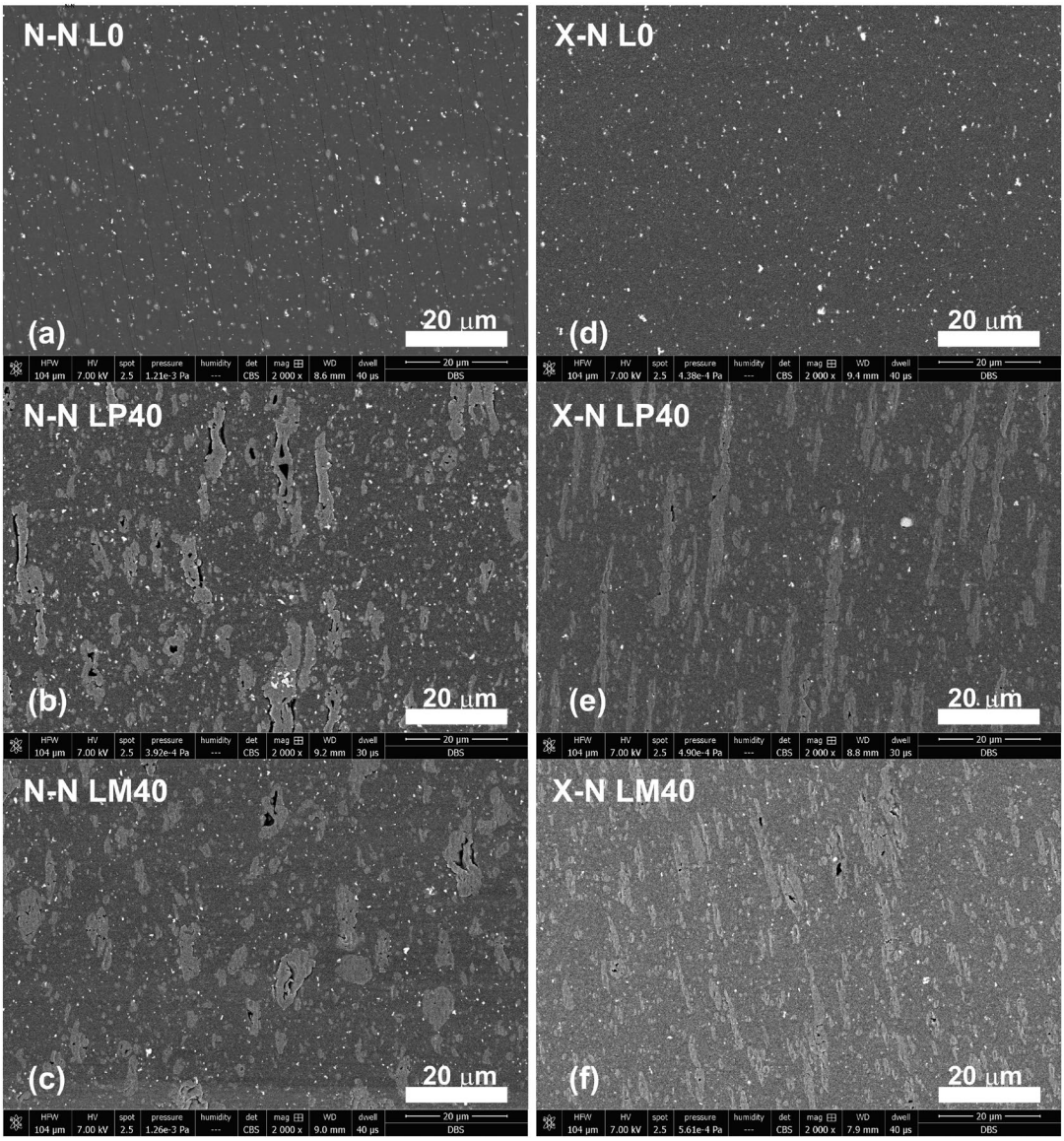

FIGURE 1 | Scanning electron microscopy of the cryo-ultramicrotomed cross-section of the rubber composites: (a) N-N L0, (b) N-N LP40, (c) N-N LM40, (d) X-N L0, (e) X-N LP40, and (f) X-N LM40 at a magnification of 2000× (scale bar of 20 µm).

lignin-filled compounds exhibit a similar morphology, characterized by irregular lignin particles that tend to be elongated and aligned in the same direction. The formation of this pattern may have occurred during the two-roll mixing mill step, which stretched and aligned the lignin particles, since lignin is a biopolymer that can be deformed during processing. However, it is clear that the lignin particles in X-N compounds are more elongated and thinner than those in the N-N samples. This finding may be attributed to the presence of carboxylic groups in XNBR, as discussed by Campos et al. [12], which improves the interaction and facilitates the incorporation of lignin into the rubber matrix. According to Campos et al. [22] demonstrate that lignin interacts with XNBR through two primary mechanisms: hydrogen bonding between lignin methoxy groups and rubber carboxylic acids, and the formation of lignin-zinc-rubber coordination complexes, as evidenced by shifts in FTIR absorbance. Also, the lignin particles are evenly distributed and exhibit adhesion to the rubber matrix. This is evident from the absence of space in the contour regions of the particles, although some particles do show internal voids. Furthermore, a slight reduction in lignin size and an improvement in its dispersion are observed for N-N LM40 (Figure 1c) and X-N LM40 (Figure 1f) compared to N-N LP40 (Figure 1b) and X-N LP40 (Figure 1e). According to Wikberg et al. [23], the kraft lignin analyzed in their study displayed a smooth surface with minimal porosity. The SEM image presented by Wang et al. [24] demonstrates a significant tendency for lignin agglomeration in NBR/lignin composites. This indicates the need to develop techniques to enhance dispersion of lignin in the rubber matrix.

The degree of dispersion was assessed by quantifying the lignin particles in SEM images. Table 2 shows the total number of particles exceeding $3\,\mu m^2$ (the smallest particle visible in the photos) and the number of larger aggregates (greater than $20\,\mu m^2$) present within a defined sample area of $20{,}000\,\mu m^2$. An illustrative example of the analysis is shown in Figure S2.

Table 2 shows that the N-N LP40 and X-N LP40 samples have 35% of particles with an area larger than $20\,mm^2$. This percentage surpasses that of the N-N LM40 and X-N LM40 composites, which show values of 27% and 23%, respectively. This result highlights a notable difference in particle size distribution between the LP40 and LM40 samples. Such variations could impact the performance properties of the composites. These results suggest that incorporating the lignin masterbatch form contributed to a reduction in particle area, leading to fewer agglomerates and enhanced dispersion of lignin particles within the rubber matrix [21].

3.2 | Vulcanization Assessment and Cross-Link Density

Figure 2 illustrates the comparison of vulcanization curves (torque vs. time) for the N-N (Figure 2a) and X-N (Figure 2b) compounds. It is evident that all lignin-filled compounds achieved higher torque values and displayed steeper curves when compared to the unfilled rubber samples. Additionally, the curves of the lignin-filled compounds overlap significantly until approximately 5 min. Table 3 shows the values of vulcanization properties.

The scorch time (t_{s1}) values show no significant differences (Table 3). This result shows that adding lignin to a rubber formulation with the effective vulcanization system (Table 1), either as a masterbatch or powder, does not significantly change t_{s1}, whose value is 2.0 ± 0.2 min. The analysis of optimal curing time (t_{90}) reveals that the unfilled rubbers demonstrate shorter t_{90} values compared to the lignin-filled compounds, suggesting that the presence of lignin may hinder the vulcanization reactions. However, this trend is not shown in Figure 2, where the vulcanization curves of the lignin-filled compounds appear to have a steeper slope than those of the unfilled rubber. Furthermore, while the vulcanization curves for unfilled rubber reach a plateau, the lignin-filled compounds exhibit marching-modulus curves, which significantly influence the determination of t_{90}. This marching modulus, also commonly seen for silica, interferes with the determination of t_{90} [21]. Therefore, in this study, we conducted a kinetics investigation using an autocatalytic model to determine whether lignin influences the vulcanization of rubber. Figure 3 and Table 4 show that the autocatalytic model fits well the experimental data of vulcanization rate ($d\alpha/dt$) versus conversion (α) for N-N (Figure 3a) and X-N (Figure 3b) compounds. Curves of the vulcanization rate ($d\alpha/dt$) versus time, S4, show the same trends as Figure 3.

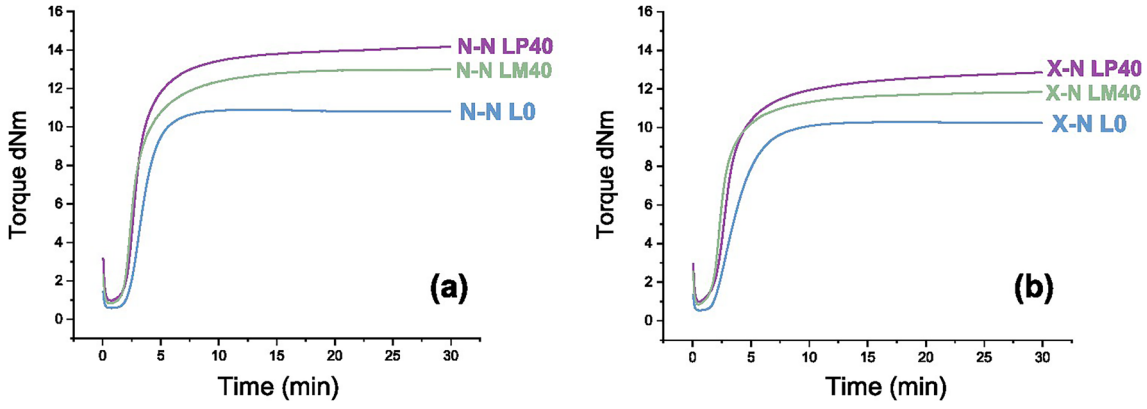

FIGURE 2 | Vulcanization curves (torque versus time) of (a) N-N and (b) X-N compounds.

TABLE 3 | Vulcanization properties.

Property	N-N L0	N-N LP40	N-N LM40	X-N L0	X-N LP40	X-N LM40
t_{s1} (min)	2.3	2.1	1.9	2.1	1.9	1.7
t_{90} (min)	5.4	7.1	7.2	6.7	8.4	6.5
ML (dNm)	0.6	1.0	0.8	0.5	1.0	0.8
MH (dNm)	10.9	14.2	13.0	10.3	12.8	11.8
ΔM (dNm)	10.3	13.2	12.2	9.7	11.9	11.0

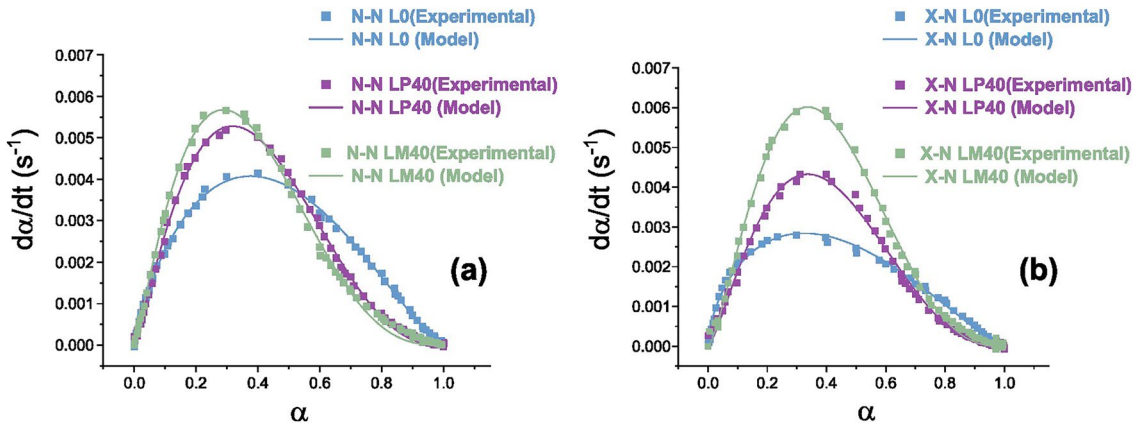

FIGURE 3 | Vulcanization rate ($d\alpha/dt$) versus conversion (a) of (c) N-N and (d) X-N compounds (dots are experimental data, and lines are the fitting of the autocatalytic model).

TABLE 4 | Autocatalytic model.

Sample code	Model	*R*-square
N-N L0	$\frac{d\alpha}{dt} = 0.017\alpha^{0.8}(1-\alpha)^{1.3}$	0.9979
N-N LP40	$\frac{d\alpha}{dt} = 0.056\alpha^{1.2}(1-\alpha)^{2.6}$	0.9979
N-N LM40	$\frac{d\alpha}{dt} = 0.069\alpha^{1.2}(1-\alpha)^{3.0}$	0.9959
X-N L0	$\frac{d\alpha}{dt} = 0.009\alpha^{0.6}(1-\alpha)^{1.3}$	0.9891
X-N LP40	$\frac{d\alpha}{dt} = 0.057\alpha^{1.4}(1-\alpha)^{2.7}$	0.9944
X-N LP40	$\frac{d\alpha}{dt} = 0.098\alpha^{1.5}(1-\alpha)^{2.9}$	0.9944

As shown in Table 4, all lignin-filled rubber compounds exhibited higher reaction rate constants (k) compared to the unfilled rubber, indicating faster vulcanization kinetics. Additionally, the reaction order ($m+n$) increased from approximately 2 for the unfilled compounds to around 4 for those filled with lignin. This evidence suggests that the addition of lignin has a significant influence on the vulcanization process. In N-N composites, lignin increased the maximum vulcanization rate and shifted its peak to slightly lower conversions, irrespective of dispersion method (LP40 vs. LM40). At higher conversions, however, the rate decreased, reflecting a "marching modulus" behavior and an increased t_{90}. A similar trend, an initial rate increase followed by a decrease, occurred in X-N composites. Here, dispersion played a key role: the superior lignin dispersion in X-N LM40 led to a higher vulcanization rate than in X-N LP40. The origin of these kinetic effects is complex. Literature often attributes filler-induced rate increases to matrix softening or improved thermal homogeneity [12].

However, data presented in Sections 3.3 and 3.4 rule out these conventional mechanisms, as lignin neither softens the matrix nor is knowns as an efficient thermal conductor. The observed acceleration may instead involve a more complex interfacial mechanism. A comparison with silica, another filler with an acidic surface known to interfere with vulcanization, underscores this complexity. For instance, even unmodified silica, which typically retards curing via accelerator adsorption, can increase the vulcanization rate under specific conditions, such as certain filler loadings [23]. Therefore, while the precise mechanism in the X-N blend requires further study, our results unequivocally demonstrate that lignin dispersion is a critical factor governing its vulcanization kinetics.

The minimum torque value (ML) indicates the stiffness of the unvulcanized compound. Therefore, the increase in ML values for the lignin-filled formulations is an expected behavior. The type of rubber used (N-N and X-N) does not significantly affect ML, regardless of lignin's presence, which can be attributed to the similar Mooney viscosities of all rubber grades employed (see Section 2.1). Both N-N LM40 and X-N LM40 compounds exhibit a 20% reduction in ML compared to their N-N LP40 and X-N LP40 counterparts.

ΔM is predominantly associated with the development of crosslinking that occurs during vulcanization [25]. Thus, it was expected that all compounds would exhibit similar ΔM values, given that the same vulcanization system was employed across

TABLE 5 | Apparent cross-link densities determined by the swelling method—total (CLD-total), covalent (CLD-covalent), and ionic (CLD-ionic).

Property	N-N L0	N-N LP40	N-N LM40	X-N L0	X-N LP40	X-N LM40
CLD-total (10^{-5} mol cm^{-3})	7.34 ± 0.01	7.52 ± 0.01	7.33 ± 0.05	9.68 ± 0.11	9.89 ± 0.35	10.08 ± 0.20
CLD-covalent (10^{-5} mol cm^{-3})	7.20 ± 0.01	6.81 ± 0.01	6.62 ± 0.08	9.06 ± 0.26	7.83 ± 0.09	7.67 ± 0.03
CLD-ionic (10^{-5} mol cm^{-3})	0.14	0.71	0.71	0.61	2.06	2.41

all formulations (see Table 1); however, this was not the case. All lignin-filled compounds showed higher ΔM values, ranging from 13% to 28% more than their unfilled rubber counterparts. This could be caused by the reinforcing effect of lignin, as it is known that reinforcing filler can increase ΔM [14]. Beyond that, the co-coagulation method caused a decrease in ΔM. This indicates that greater lignin dispersion causes a decline in cross-link density.

Table 5 shows the apparent cross-link densities determined using the swelling method, presented as the total cross-link density (CLD-total), the covalent portion (CLD-covalent), and the ionic cross-link contributions (CLD-ionic). Note that the CLD values for the filled composites do not reflect their true cross-link density, because the impact of lignin on the swelling of rubber is not quantified. Elastomer chains that have a high adhesion to filler particles do not swell as much, causing an overestimation of cross-link density by swelling [17, 26]. So, the cross-link density of filled formulations is considered apparent and compared only qualitatively.

The lignin-filled compounds exhibited apparent CLD-Total values comparable to those of the unfilled rubber. However, the presence of lignin actually caused a reduction in the CLD-Covalent, even more when co-coagulated, confirming the trend observed by the ΔM. Interestingly, there was an increase in CLD-ionic of lignin-filled compounds compared to unfilled rubber. According to Zhang et al. [11], lignin can act as a natural ligand in forming zinc-based coordination bonds in XNBR. These bonds arise between zinc ions (from ZnO) and specific functional groups, such as carboxylate groups found in XNBR. The bond with XNBR is strengthened further with the addition of ZnO, creating a complex of Zn^{2+} with acrylonitrile. This results in a dual-cross-linking network composed of sulfur covalent bonds and dynamic sacrificial coordination bonds. The presence of carboxylic and phenolic groups in lignin should be considered since these groups can potentially form ionic bonds, creating a more cohesive network that restricts solvent penetration into the rubber matrix. However, further experimental tests are necessary to confirm this hypothesis.

3.3 | Payne Effect

Figure 4 shows the comparison of complex shear modulus (G^*) versus strain curves for all samples before and after vulcanization (Figure 4a,c, respectively). The G^* curves for X-N LP40 and N-N LP40, as well as for X-N LM40 and N-N LM40, are seen to overlap for the samples that haven't been vulcanized (Figure 5a). On the other hand, Figure 4b illustrates that all vulcanized samples exhibited a significant increase in G*, with no overlap among the curves. Overall, the G^* curves for X-N compounds are consistently higher than those for N-N compounds, and the curves for compounds with powdered lignin (LP) surpass those that utilize masterbatch lignin (LM). The observed differences can be attributed to the enhanced interactions between lignin and XNBR and to higher values of apparent CLD-Total (Table 5), along with the distinct morphologies of lignin within the rubber matrix, as discussed in Section 3.1.

The Payne effect is a phenomenon observed in rubber compounds filled with carbon black or silica. It is characterized by a decrease in the complex modulus (G^*) or elastic modulus (G') when the material undergoes cyclic or dynamic deformation at low levels. This effect occurs due to the breakdown of the filler network, as the filler particles remain rigid and do not deform [19, 27, 28]. In this study, we applied the same principle for evaluating the Payne effect. Specifically, at the test temperature (60°C), lignin remains rigid and does not undergo deformation during strain sweep testing.

Figure 4 indicates that the rubber compounds with powdered lignin show a more pronounced Payne effect than those with masterbatch lignin, for both uncured and cured compounds. This suggests that incorporating lignin through the masterbatch method leads to a reduced filler-network. The behavior observed for the Payne effect in this study agrees with Kazemi et al. [29] and Campos et al. [12]. Kazemi et al. [29] stated that lignin raises the Payne effect of unvulcanized NR compounds, suggesting that it contributes to the formation of filler networks. Campos et al. [12] found that the Payne effect of vulcanized XNBR depends on the amount of lignin, getting stronger as the lignin content rises. According to Fröhlich et al. [19], the magnitude of the Payne effect is a result of the stability of filler–filler and filler–polymer interactions, which determine the extent of the filler–filler percolation network and its ability to resist cyclic deformation. Increases in filler concentration and filler-specific surface area generally lead to greater filler-filler interactions, resulting in a stronger network and, consequently, a greater magnitude of the Payne effect. Although dispersion with masterbatch lignin improved, the Payne effect did not increase; rather, it decreased. While this behavior remains under investigation, the co-coagulation method may have led to an increased dispersion and more stable filler-filler interactions. Nevertheless, it seems that the Payne effect interpretation cannot be done the same way for lignin as it is done for carbon black and silica. Possible reasons include the wide range of lignin particle morphology, the in-rubber structure of lignin, and the nature of the polymer–filler interaction between lignin and XNBR.

3.4 | Mechanical Properties

Figure 5 illustrates the stress versus strain curves of one representative specimen from each of unfilled NBR and XNBR and

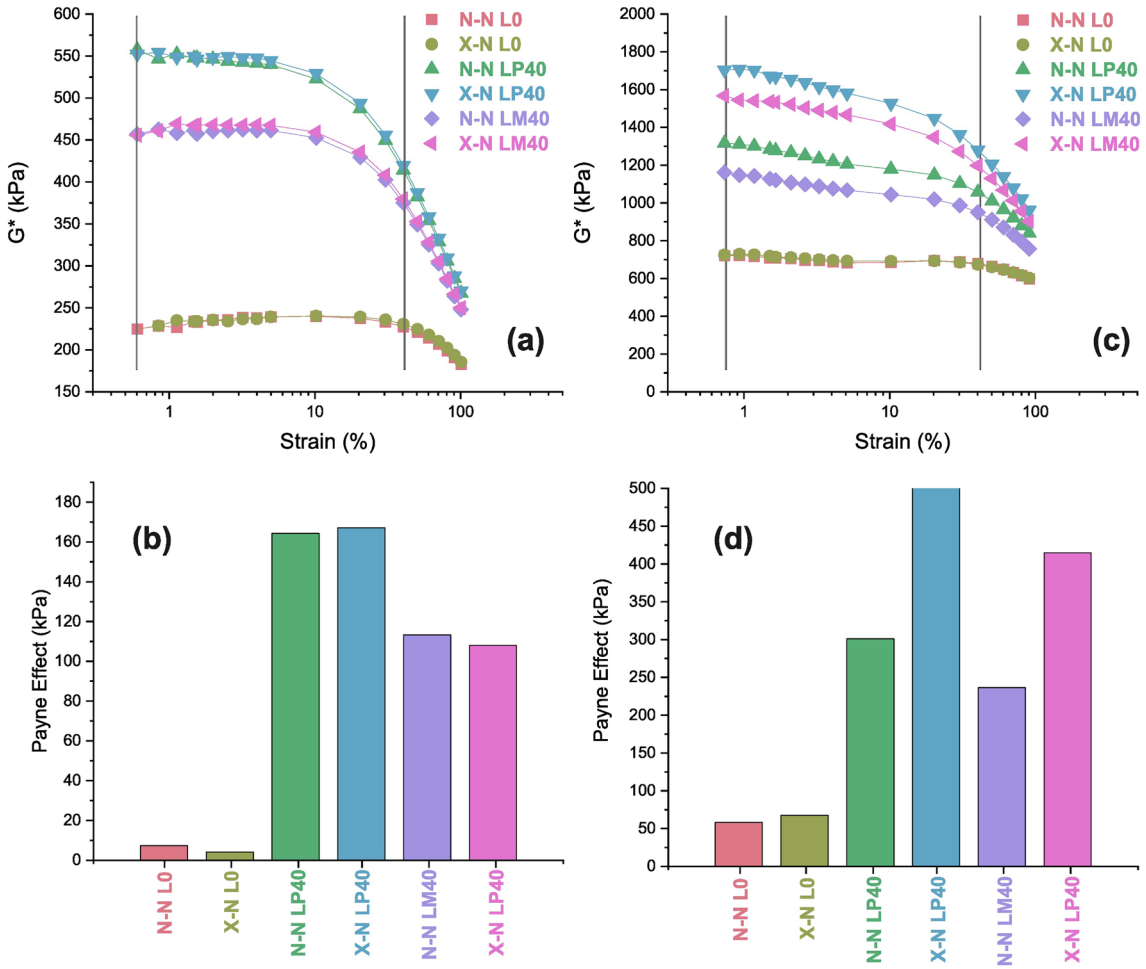

FIGURE 4 | *G** versus strain curves and Payne effect comparison of unvulcanized (a, b) and vulcanized (c, d) rubber compounds.

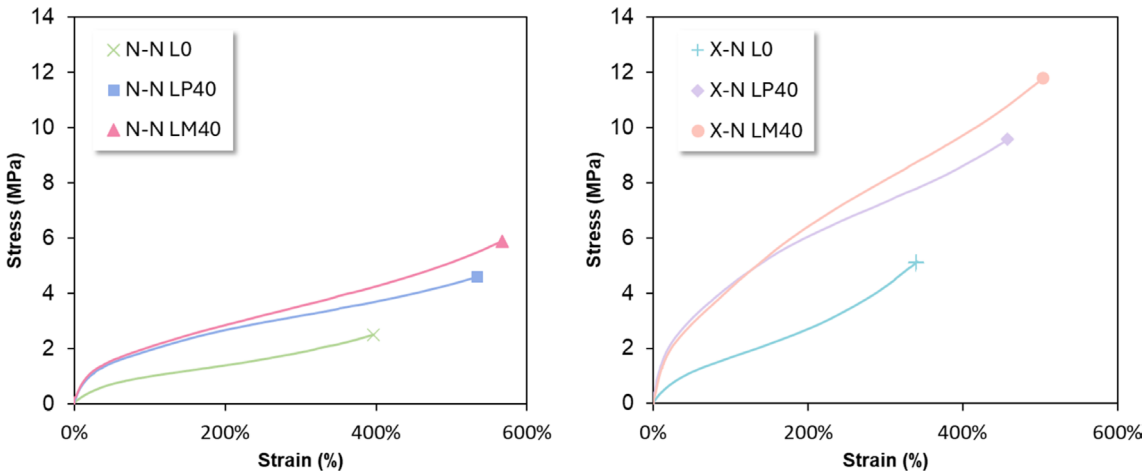

FIGURE 5 | Stress–strain curves for N-N and X-N rubber composites (each curve representing a single specimen).

lignin-filled composites for comparison purposes. It is evident that all composites demonstrate typical low-stress, high-deformation profiles, undergoing significant elastic deformation prior to failure.

Table 6 shows the mean and standard deviation values for stress at 100% strain (or modulus at 100%), tensile strength, elongation at break, tear strength, and Shore A hardness data. A one-way ANOVA revealed p values <0.05 for these mechanical properties, indicating statistical differences among the composites. Post hoc analysis using Fisher's least significant difference (LSD) procedure, indicated by letters in Table 6, shows that samples sharing the same letter do not significantly differ in these mechanical properties. Additionally, all Cochran tests yielded p values >0.05 for these properties, indicating the homogeneity of variances.

TABLE 6 | The mean values and standard deviation (in parentheses) for stress at 100% of strain, tensile strength, elongation at break, tear strength, and Shore A hardness of the unfilled NBR and XNBR and lignin-filled composites.

Code	Stress at 100% (MPa)	Tensile strength (MPa)	Elongation at break (%)	Hardness Shore A	Tear strength (kNm^{-1})
N-N L0	1.10[a] (0.01)	2.5[a] (0.1)	380[a] (19)	48[a] (0)	16.6[a] (1.7)
N-N LP40	1.91[b] (0.03)	4.7[b] (0.2)	541[b] (19)	61[b] (0)	34.3[b] (1.5)
N-N LM40	2.08[b] (0.04)	5.9[c] (0.1)	567[b] (7)	58[b] (0)	36.3[b] (1.5)
X-N L0	1.64[c] (0.01)	5.5[d] (0.2)	355[a] (13)	55[c] (0)	26.7[c] (1.5)
X-N LP40	4.33[d] (0.04)	9.1[e] (0.2)	437[c] (16)	73[d] (0)	56.0[d] (1.5)
X-N LM40	4.41[d] (0.09)	11.7[f] (0.1)	494[c] (8)	72[d] (0)	61.6[e] (1.5)

Note: The superscript with the same letter denotes that the difference between the means is not statistically significant based on Fisher's least significant difference (LSD) procedure. All one-way ANOVAs produced p values < 0.05. All Cochran tests produced p values > 0.05.

Compared to N-N L0, the X-N L0 demonstrates superior stress at 100% and enhanced tensile strength, while exhibiting similar elongation at break (Table 6). Furthermore, X-N L0 also has higher Shore A hardness and tear strength than N-N L0. This behavior can be attributed to the higher CLD-ionic of X-N L0 ($0.61\,mol\,cm^{-3}$) compared to that of N-N L0 ($0.14\,mol\,cm^{-3}$).

Regarding lignin-filled compounds, the addition of 40 phr of lignin increases the stress at 100% by approximately 80% for all-NBR compounds (N-N LP40 and N-N LMP40) and by 160% for XNBR/NBR compounds (X-N LP40 and X-N LMP40). No significant differences in the stress at 100% were observed based on the method used for lignin incorporation. This finding shows the role of lignin in enhancing this mechanical property, which is in accordance with the literature [12, 30].

All composites have different tensile strengths (Table 6). For instance, the composites made with masterbatch show an increase of 26% (N-N LM40) and 29% (X-N LM40) compared to the similar formulations made with powder lignin (N-N LP40 and X-N LP40). This increase in tensile strength for N-N LM40 and X-N LM40 can be attributed to better dispersion of the filler in the masterbatch form, as shown by the SEM analysis (Figure 1). Furthermore, compared to their respective unfilled rubber counterparts, N-N LM40 (136%) and X-N LM40 (113%) exhibit the highest enhancements in tensile strength. Our findings align with Campos et al. [12], who observed that as the lignin content increased, so did the tensile strength. In contrast, studies on NBR filled with lignin, such as those by Agarwal et al. [30] and Setua et al. [31], reported a decrease in tensile strength, which is a behavior different from what we observed. Agarwal et al. [30] attributed their results to a decrease in crosslink density and the difference in the hydrophobicity between lignin and NBR. In our study, an increase in tensile strength is observed with the addition of 40 phr of lignin, with this increase being more significant for N-N LM40 (Table 6), even though a decrease in CLD was also detected. The improvement in this property likely occurred due to the better dispersion of lignin in the rubber matrix (Figure 1), which may have resulted in better interfacial interaction between the lignin and the rubber matrix, increasing the mechanical reinforcement.

Table 6 and Figure 5 show that all the lignin-filled composites exhibited greater elongation at break compared to the unfilled rubber. Furthermore, the X-N compounds exhibited less elongation than N-N. Zhang et al. [11] suggest that the ionic and coordination bonds present in zinc within XNBR can function as sacrificial bonds, dissipating energy during elongation by breaking down. However, our study found no significant difference in the elongation at break between the N-N L0 and X-N L0 samples, as determined by Fisher's least significant difference procedure (Table 6). On the other hand, as shown in Table 5, lignin plays a role in reducing the CLD-Covalent values while increasing the CLD-Ionic values, which can influence the material's elongation. This leads to the hypothesis that the elongation at break for lignin-filled compounds may be attributed to the reduction of CLD-covalent and the participation of lignin in CLD-ionic. This interaction creates a network that distributes stress more evenly during deformation, ultimately enhancing elongation. These ionic bonds reinforce the structure and provide the polymer chains with increased mobility.

Table 6 shows an increase in tear resistance of around 120% for the lignin-filled compounds in comparison with unfilled rubber, with the enhancement being more pronounced for X-N LM40. Campos et al. [12] observed that the addition of lignin resulted in an increase in the tear strength of XNBR compounds. On the other hand, Agarwal et al. [30] did not notice any difference in tear resistance in NBR/lignin compounds. This improvement observed in our study can be attributed to the balance between the lignin-lignin network, lignin-rubber interaction, and the size and distribution of lignin in the rubber matrix. The presence of fillers increases the tear strength of a rubber matrix through the breakdown of the filler network, the yield of bound rubber on the filler surfaces, and friction between filler and rubber molecules. Furthermore, the dispersed particles deflect or arrest growing cracks [32].

Shore A hardness varies depending on the type of rubber, showing higher values for the X-N blend (Table 6). As expected, the addition of 40 phr of lignin contributes to an increase in hardness. Furthermore, there is no difference between N-N LP40 and N-N LM40, as well as between X-N LP40 and X-N LM40, indicating that the methods used to add lignin to the rubber do not affect the hardness.

4 | Conclusion

This study demonstrates that the method of incorporating lignin, along with the presence of XNBR, significantly affects

the morphology of the lignin particle, vulcanization behavior, covalent and ionic crosslink formations, intensity of the Payne effect, and mechanical properties performance. The SEM analysis reveals that lignin particles are uniformly distributed throughout the rubber matrix, exhibiting a morphology characterized by irregular shapes and aligned in the same direction. For composites with an NBR/XNBR blend, the lignin particles appear thinner and more elongated compared to those found in NBR compounds. Compounds that utilize lignin in a masterbatch show a slight reduction in particle size and improved dispersion compared to those with powdered lignin.

The crosslink density and vulcanization properties were highly affected by the addition of lignin. The compounds with filler exhibited higher torque values, with the ΔM values ranging from 13% to 28% more than their unfilled rubber counterparts. In this context, particular attention is given to the proportion between covalent and ionic crosslinks. The incorporation of lignin markedly influences the vulcanization process by modifying the balance between covalent and ionic crosslink densities, which consequently affects the mechanical and dynamic properties of the resulting composites. It is also worth mentioning that the lignin-filled composites exhibited higher reaction rate constant values compared to the unfilled NBR. This behavior was attributed to the smaller particle size of the masterbatch lignin compositions, as well as to the improved dispersion of lignin within the rubber matrix. Additionally, these observed differences in the morphologies of lignin particles influence the intensity of the Payne effect: that is, there is a more pronounced Payne effect for rubber composites that are made with powdered lignin.

The rubber/lignin composites produced in this study demonstrated advantages over unfilled rubber, with the addition of lignin increasing properties such as tensile strength, stress at 100%, elongation at break, and tear strength. These findings suggest that lignin acts as a reinforcing agent, enhancing the material's resistance to crack propagation under stress. The effect on properties was more pronounced in composites with an NBR/XNBR blend, owing to the stronger interaction of XNBR with lignin. The most notable improvements occurred in composites where lignin was incorporated as a masterbatch, due to the better dispersion within the elastomeric matrix.

Author Contributions

Nicoly Rosario da Costa: conceptualization, methodology, investigation, formal analysis, writing – original draft. **Gustavo Ninho Campos:** conceptualization, investigation, writing – original draft, methodology, formal analysis. **Elisson Brum Dutra da Rocha:** writing – review and editing, funding acquisition, conceptualization, supervision. **João Paulo Cosas Fernandes:** conceptualization, funding acquisition, writing – review and editing, supervision. **Ana Maria Furtado de Sousa:** conceptualization, funding acquisition, writing – review and editing, supervision.

Acknowledgments

The authors would like to thank Suzano S.A. for donating the lignin and Nitriflex S.A. Industria e Comércio for donating the raw materials and the MSc scholarship received by Nicoly Rosario da Costa. The authors would like to thank the research support received from Coordenação de Aperfeiçoamento de Pessoal de Nível Superior—CAPES [Financing code 001: PhD Scholarship received by Nicoly Rosario da Costa], Fundação de Amparo à Pesquisa do Estado do Rio de Janeiro—FAPERJ [E-26/200.289/2021: PhD Scholarship received by Gustavo Ninho Campos and SEI-260003/006163/2024-APQ1: received by Ana Maria Furtado de Sousa], and Conselho Nacional de Desenvolvimento Científico e Tecnológico—CNPQ [PQ-2:304054/2025-9 received by Ana Maria Furtado de Sousa]. The authors acknowledge the NanoBio-ICMG Platform (UAR 2607, Grenoble) for granting access to the electron microscopy facilities.

Funding

This work was supported by- Fundação Carlos Chagas Filho de Amparo à Pesquisa do Estado do Rio de Janeiro (E-26/200.289/2021 and SEI-260003/006163/2024-APQ1), Coordenação de Aperfeiçoamento de Pessoal de Nível Superior (001), and Conselho Nacional de Desenvolvimento Científico e Tecnológico (PQ-2:304054/2025-9).

Conflicts of Interest

The authors declare no conflicts of interest.

Data Availability Statement

Data from this study are available from the corresponding author upon request.

References

1. S. Fadlallah, P. Sinha Roy, G. Garnier, K. Saito, and F. Allais, "Are Lignin-Derived Monomers and Polymers Truly Sustainable? An In-Depth Green Metrics Calculations Approach," *Green Chemistry* 23, no. 4 (2021): 1495–1535, https://doi.org/10.1039/D0GC03982A.

2. D. Kai, M. J. Tan, P. L. Chee, Y. K. Chua, Y. L. Yap, and X. J. Loh, "Towards Lignin-Based Functional Materials in a Sustainable World," *Green Chemistry* 18, no. 5 (2016): 1175–1200, https://doi.org/10.1039/C5GC02616D.

3. K. Roy, S. C. Debnath, and P. Potiyaraj, "A Review on Recent Trends and Future Prospects of Lignin Based Green Rubber Composites," *Journal of Polymers and the Environment* 28, no. 2 (2020): 367–387, https://doi.org/10.1007/s10924-019-01626-5.

4. B. P. Chang, A. Gupta, R. Muthuraj, and T. H. Mekonnen, "Bioresourced Fillers for Rubber Composite Sustainability: Current Development and Future Opportunities," *Green Chemistry* 23, no. 15 (2021): 5337–5378, https://doi.org/10.1039/D1GC01115D.

5. M. Fumagalli, J. Berriot, B. de Gaudemaris, et al., "Rubber Materials From Elastomers and Nanocellulose Powders: Filler Dispersion and Mechanical Reinforcement," *Soft Matter* 14, no. 14 (2018): 2638–2648, https://doi.org/10.1039/C8SM00210J.

6. T. Higuchi, "Look Back Over the Studies of Lignin Biochemistry," *Journal of Wood Science* 52, no. 1 (2006): 2–8, https://doi.org/10.1007/s10086-005-0790-z.

7. J. Liu, X. Li, M. Li, and Y. Zheng, "Lignin Biorefinery: Lignin Source, Isolation, Characterization, and Bioconversion," *Advances in Bioenergy* 7 (2022): 211–270, https://doi.org/10.1016/bs.aibe.2022.05.004.

8. N. A. Mohamad Aini, N. Othman, M. H. Hussin, K. Sahakaro, and N. Hayeemasae, "Lignin as Alternative Reinforcing Filler in the Rubber Industry: A Review," *Frontiers in Materials* 6 (2020): 6, https://doi.org/10.3389/fmats.2019.00329.

9. M. Li, L. Zhu, H. Xiao, et al., "Design of a Lignin-Based Versatile Bioreinforcement for High-Performance Natural Rubber Composites," *ACS Sustainable Chemistry & Engineering* 10, no. 24 (2022): 8031–8042, https://doi.org/10.1021/acssuschemeng.2c02113.

10. P. Sekar, J. W. M. Noordermeer, R. Anyszka, H. Gojzewski, J. Podschun, and A. Blume, "Hydrothermally Treated Lignin as a Sustainable Biobased Filler for Rubber Compounds," *ACS Applied Polymer Materials* 5, no. 4 (2023): 2501–2512, https://doi.org/10.1021/acsapm.2c02170.

11. G. Zhang, C. Tian, J. Shi, et al., "Mechanically Robust, Self-Repairable, Shape Memory and Recyclable Ionomeric Elastomer Composites With Renewable Lignin via Interfacial Metal–Ligand Interactions," *ACS Applied Materials & Interfaces* 14, no. 33 (2022): 38216–38227, https://doi.org/10.1021/acsami.2c10731.

12. G. N. Campos, E. B. D. da Rocha, C. R. G. Furtado, M. A. G. de Figueiredo, and A. M. F. de Sousa, "Using Carboxyl Groups to Improve the Compatibility of XNBR/Lignin Composites," *Polymer Composites* 45 (2024): 4124–4137, https://doi.org/10.1002/pc.28047.

13. A. Moaddab, M. Kalaee, S. Mazinani, A. Aghajani, and M. M. Rajab, "Cure Kinetics and Final Performance of Styrene Butadiene Styrene Block Copolymer/Silica Nanocomposites," *Rubber Chemistry and Technology* 88, no. 1 (2015): 53–64, https://doi.org/10.5254/rct.14.85974.

14. M. Raef, S. M. Hosseini, M. Nabavian Kalat, and M. Razzaghi-Kashani, "Vulcanization Kinetics of Styrene Butadiene Rubber Reinforced by Graphenic Particles," *SPE Polymers* 2, no. 2 (2021): 122–133, https://doi.org/10.1002/pls2.10039.

15. P. J. Flory and J. Rehner, "Statistical Mechanics of Cross-Linked Polymer Networks I. Rubberlike Elasticity," *Journal of Chemical Physics* 11, no. 11 (1943): 512–520, https://doi.org/10.1063/1.1723791.

16. G. N. Campos, A. C. R. Coimbra, A. A. da Silva, et al., "Cross-Link Density Measurement of Nitrile Rubber Vulcanizates Using Dynamic Shear Test," *Polímeros* 32, no. 1 (2022): 1–6, https://doi.org/10.1590/0104-1428.20220031.

17. G. Delahaye, A. Redon, B. Ruellan, et al., "A Comprehensive Review on Active Chain Density Evaluation From Swelling and Insights for Better Accounting for Insoluble Particles," *Journal of Applied Polymer Science* 141, no. 35 (2024): 1–19, https://doi.org/10.1002/app.55899.

18. C. Xu, L. Cao, B. Lin, X. Liang, and Y. Chen, "Design of Self-Healing Supramolecular Rubbers by Introducing Ionic Cross-Links Into Natural Rubber via a Controlled Vulcanization," *ACS Applied Materials & Interfaces* 8, no. 27 (2016): 17728–17737, https://doi.org/10.1021/acsami.6b05941.

19. J. Fröhlich, W. Niedermeier, and H. D. Luginsland, "The Effect of Filler–Filler and Filler–Elastomer Interaction on Rubber Reinforcement," *Composites. Part A, Applied Science and Manufacturing* 36, no. 4 (2005): 449–460, https://doi.org/10.1016/j.compositesa.2004.10.004.

20. T. Xia, A. M. Wemyss, R. Salehiyan, et al., "Effective and Fast-Screening Route to Evaluate Dynamic Elastomer-Filler Network Reversibility for Sustainable Rubber Composite Design," *ACS Sustainable Chemistry & Engineering* 11, no. 50 (2023): 17857–17869, https://doi.org/10.1021/acssuschemeng.3c06752.

21. J. Koskinen, N. Kemppainen, and E. Sarlin, "Lignin Dispersion in Polybutadiene Rubber (BR) With Different Mixing Parameters," *Progress in Rubber, Plastics and Recycling Technology* 41, no. 4 (2024): 468–482, https://doi.org/10.1177/14777606241281619.

22. G. N. Campos, E. B. D. da Rocha, K. Paiva, et al., "Mechanical Performance Under Compressive Load of Carboxylated Nitrile Rubber and Kraft Lignin Composites," *Polymer Composites* 0: (2025): 1–11, https://doi.org/10.1002/pc.70403.

23. H. Wikberg, T. Ohra-Aho, F. Pileidis, and M. M. Titirici, "Structural and Morphological Changes in Kraft Lignin During Hydrothermal Carbonization," *ACS Sustainable Chemistry & Engineering* 3, no. 11 (2015): 2737–2745, https://doi.org/10.1021/acssuschemeng.5b00925.

24. H. Wang, W. Liu, J. Huang, D. Yang, and X. Qiu, "Bioinspired Engineering Towards Tailoring Advanced Lignin/Rubber Elastomers," *Polymers* 10, no. 9 (2018): 1033, https://doi.org/10.3390/polym10091033.

25. Z. S. Shashok, E. P. Uss, A. Y. Lyushtyk, S. N. Kayushnikov, and O. V. Stoyanov, "Vulcanization of Elastomer Compositions With Silicon Acid Fillers," *Polymer Science, Series D* 17, no. 2 (2024): 236–241, https://doi.org/10.1134/S1995421224700394.

26. G. Kraus, "Swelling of Filler-Reinforced Vulcanizates," *Journal of Applied Polymer Science* 7, no. 3 (1963): 861–871, https://doi.org/10.1002/app.1963.070070306.

27. A. D. Drozdov and A. Dorfmann, "The Payne Effect for Particle-Reinforced Elastomers," *Polymer Engineering and Science* 42, no. 3 (2002): 591–604, https://doi.org/10.1002/pen.10974.

28. R. Yang, Y. Song, and Q. Zheng, "Payne Effect of Silica-Filled Styrene-Butadiene Rubber," *Polymer (Guildf)* 116 (2017): 304–313, https://doi.org/10.1016/j.polymer.2017.04.003.

29. H. Kazemi, F. Mighri, K. W. Park, S. Frikha, and D. Rodrigue, "Natural Rubber Biocomposites Reinforced With Cellulose Nanocrystals/Lignin Hybrid Fillers," *Polymer Composites* 43, no. 8 (2022): 5442–5453, https://doi.org/10.1002/pc.26846.

30. K. Agarwal, M. Prasad, R. B. Sharma, and D. K. Setua, "Novel Bio-Degradable Lignin Reinforced NBR Composites," *Novel Bio-Degradable Lignin Reinforced NBR Composites* 4 (2014): 47, https://www.researchgate.net/publication/298173634.

31. D. K. Setua, M. K. Shukla, V. Nigam, H. Singh, and G. N. Mathur, "Lignin Reinforced Rubber Composites," *Polymer Composites* 21, no. 6 (2000): 988–995, https://doi.org/10.1002/pc.10252.

32. M. Alimardani and M. Razzaghi-Kashani, "The Correlation of Tear Deviation and Resistance With the Bound Rubber Content in Rubber-Silica Composites," *Polymer Testing* 90 (2020): 106762, https://doi.org/10.1016/j.polymertesting.2020.106762.

Supporting Information

Additional supporting information can be found online in the Supporting Information section. **Figure S1:** Standard curve for determining the actual amount of lignin in masterbatches. **Figure S2:** Rubber composites agglomerate quantification of (a) N-N L0, (b) N-N LP40, (c) N-N LM40, (d) X-N L0, (e) X-N LP40, and (f) X-N LM40 at a magnification of 2000× (scale bar of 20 μm). **Figure S3:** Vulcanization rate (da/dt) versus time of (a) N-N and (b) X-N compounds (dots are experimental data).